Polymer Bulletin (2022) 79:4069–4097
https://doi.org/10.1007/s00289-021-03659-0

ORIGINAL PAPER

Fabrication and characterization of coblended methyl cellulose with polyvinyl alcohol electrospun nanofibers as a carrier for drug delivery system

Bindu Kumari N. Yadav[1] · Gayatri C. Patel[1]

Received: 27 July 2020 / Revised: 26 November 2020 / Accepted: 5 March 2021 /
Published online: 20 April 2021

Abstract

Polymeric nanofibers have gained a great deal of attention in recent years. This study aims to produce and evaluate a methylcellulose (MC) and polyvinyl alcohol (PVA) based nanofibers mat using the electrospinning process. 2^{5-2} fractional factorial screening design has been used to study the effect of critical formulation and process parameters, such as concentration of MC (%), the concentration of PVA (%), applied Voltage (kV), distance (cm), flow rate (ml/hr) on the critical quality attributes like fiber diameter, tensile strength, and morphology. The fiber morphology and fiber diameter of nanofibers were investigated by scanning electron microscopy (SEM).s The optimized nanofibers mat was further characterized by Fourier transform infrared (FTIR) spectroscopy, Differential scanning electrons (DSC), Thermal gravimetric analysis (TGA), X-ray diffraction (XRD), Atomic force microscopy (AFM). Parameters such as contact angle and rate of biodegradation were studied for an optimized batch. The SEM results showed the uniform morphology of optimized nanofibers without beads with fiber diameter in the range of 100–200 nm. FTIR analysis demonstrated good intermolecular interactions between the molecules of MC with PVA. DSC-TGA study showed good thermal properties of nanofibers. XRD study showed the crystalline nature of nanofibers. Maximum tensile strength up to 2.74 Mpa was obtained which is desired for drug delivery application. The exaggeration of the fiber diameter was measured by AFM and found good surface morphology. Furthermore, results of contact angle and biodegradation rate proved that prepared nanofibers would be considered as a suitable carrier for controlled drug delivery applications like wound healing.

✉ Gayatri C. Patel
gayatripatel26@gmail.com

[1] Department of Pharmaceutics and Pharmaceutical Technology, Charotar University of Science and Technology, Ramanbhai Patel College of Pharmacy, CHARUSAT Campus, Changa-388 421, Anand, Gujarat, India

Graphic abstract

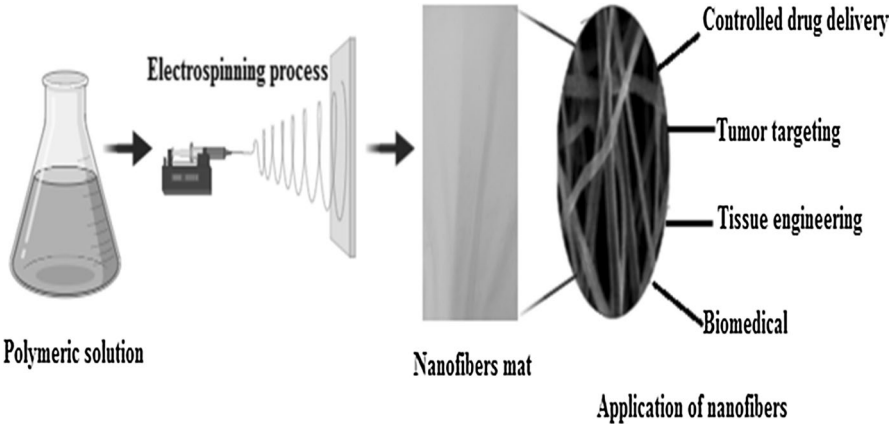

Keywords Methyl cellulose · Nanofibers mat · 2^{5-2} fractional factorial design · Morphology · Drug delivery

Abbreviations

MC	Methyl cellulose
PVA	Poly vinyl Alcohol
PCL	Polycaprolactone
PVP	Polyvinylpyrrolidone
NFs	Nanofiber
KBr	Potassium Bromide
Wt	Weight
µg	Micro gram
Mg	Milligram
G	Gram
mL	Milliliter
Mm	Millimeter
Cm	Centimeter
sec.	Second
min.	Minute
hr.	Hours
°C	Degree centigrade
%	Percentage
±	Plus or Minus
e.g.	For example
Sr. No.	Serial number
DSC	Differential scanning calorimetry
TGA	Thermogravimetry analysis
Nm	Nanometer

RH	Relative Humidity
SEM	Scanning Electron Microscope
FTIR	Fourier Transmittance Infrared
AFM	Atomic force microscopy

Introduction

Research on therapeutic nanocarriers has received a lot of popularity over the last decade due to support from researchers working in government and private organizations. Amongst all nanocarriers studied, polymeric nanofibers (NFs) have gained a lot of interest in drug delivery applications such as tumor targeting, wound dressing, biomedical and tissue engineering applications due to their ease of fabrication, variety of biopolymer availability, and high drug loading capacity [1, 2]. NFs is an ideal drug delivery system for various pharmaceutical applications as it possesses specific properties such as high surface area, porosity and fiber diameter, and controlled drug delivery [3, 4]. NFs loaded with drugs reduce the dose as compared to conventional formulations used topically for the treatment of disease [5].

Various methods are reported for the fabrication of NFs such as electrospinning process, template synthesis, phase separation, self-assembly [6].The electrospinning method is widely used in the fabrication of NFs in drug delivery due to its ease of processing and cost-effectiveness across all the methods. The electrospinning method works on the principle of the Taylor cone effect which produces electrostatic forces resulting in the formation of fine filaments from a polymer solution [7, 8]. Numerous research demonstrated NFs approach for cell attachment and proliferation, due to its dimensions similar to a native extra cellular matrix (ECM) and mimic its fibrillary structure, which provides significant care for cellular organization and survival functions [9, 10].

In this study, an attempt has been made to develop a NFs mat using biocompatible and biodegradable polymer such as methyl cellulose (MC) and polyvinyl alcohol (PVA)which is recommended by FDA for their use in various pharmaceutical applications [11].MC is a non-ionic polymer with a glucosidic relationship of β (1–4), established together with H-bonds. It is biocompatible, cost-effective, and widely used in pharmaceutical and wound healing applications [12]. MC has been combined with the water-soluble PVA to improve mechanical strength. PVA is biodegradable, biocompatible and widely used synthetic polymer for various drug delivery applications. Several studies have been reported based on the PVA NFs mat using the electrospinning process. PVA improves cellulose polymer spin capacity and also improves the mechanical strength of plain cellulose NFs [13, 14]. Electrospinning method was employed to fabricate MC co-blended with PVA NFs mat. Optimization of NFs mat was performed using the experimental design. Selection of solvent (water: IPA) and its proportion for the fabrication of NFs in order to get tailored mechanical properties has considered as the novelty of present work. Patient acceptability, ease of application, quality parameter such as morphology, fiber diameter, tensile strength and thickness were taken into consideration for the target product profile. Quality elements were characterized and controlled as critical quality

attributes. Optimized NFs were evaluated for mechanical properties, contact angle and rate of biodegradation studies. It was also characterized by scanning electron microscopy (SEM), Fourier-transform infrared spectroscopy (FTIR), differential calorimetry scanning (DSC), thermal gravimetric analysis (TGA), tensile strength analyzer, atomic force microscopy (AFM), contact angle and rate of biodegradation.

Materials and methodology

Materials

METHOCEL™A4M methyl cellulose (viscosity of 2% solution at 20 °C, 4000 mPa.s, degree of polymerization 1400, and Mw = 270,000 kDa) was procured from Dow chemical Pvt Ltd, the Netherland, Poly (vinyl alcohol) (viscosity of 4% solution at 20 °C, 4.8—5.8 mPa.s and Mw = 1,80,000 kDa) was procured from Loba Chemie Pvt. Ltd Mumbai, Chitosan grade S (deacetylation value 80–90%, Mw = 170 kDa) was procured from Chitinor AS Norway, USA. Poly (vinyl) pyrrolidone (PVP K30) (viscosity of 5% solution at 25 °C, 2.3—2.4 mPa.s, Mw = 40,000 kDa), was procured from Loba Chemie Pvt. Ltd Mumbai, Polycaprolactone (PCL) (viscosity of 1.5% solution at 25 °C, 1.5 dL/g and Mw = 80,000 kDa) was procured from Sigma-Aldrich chemicals company, USA. E- Spin Electrospinning (E-Spin Nanotech Super ES-2, Schimadzu, Japan) was used to fabricate NFs. All other chemicals and solvents were obtained in a pure form.

Method

Preliminary trials on polymers and solvents

From the literature review and prior experience natural polymers such as MC, Chitosan and synthetic polymers such as PVA, PCL, and Poly (vinyl pyrrolidone) (PVP) were studied for the fabrication of NFs [15, 16]. For the selection of solvent, properties such as conductivity, surface tension, boiling point, dielectric constant, and viscosity were considered (Fig. 1).

Preparation of polymeric solutions for electrospinning process

The polymeric solution was prepared with continuous stirring for 2 h and kept overnight at room temperature until a clear solution was obtained. Electrospinning machine (E-Spin Nanotech SuperES-2, Schimadzu, Japan) was used to fabricate the NFs. The solution was filled into a glass syringe of size 10 ml with the flat end metal needle (18 gauge), and voltage was applied. The stationary collector with the aluminum foil enfolded was positioned at the distance from the needle tip. The electrospun NFs was removed carefully and stored till further analysis [17, 18]. The ambient temperature for the electrospinning process was 32 °C. The ambient temperature and humidity influence the viscosity of the solution and the rate of solvent

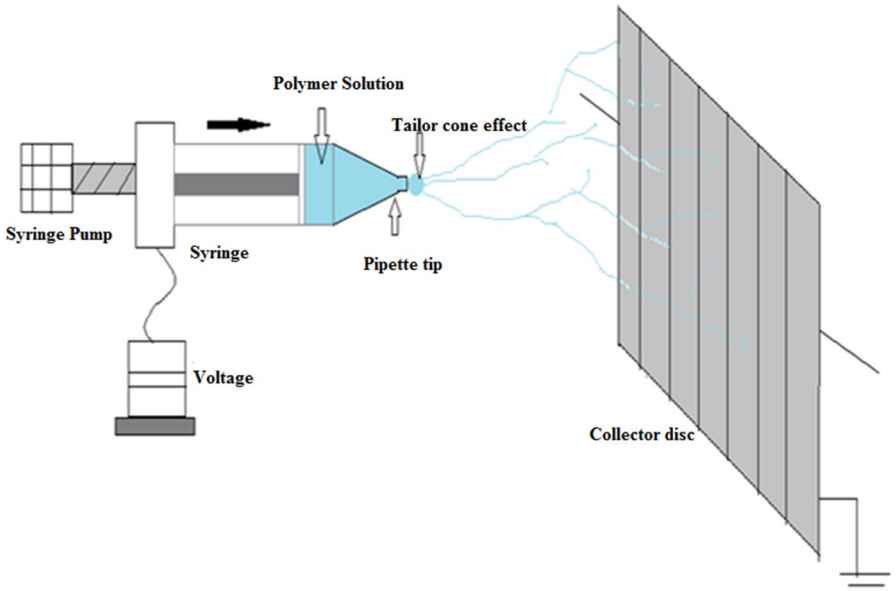

Fig. 1 Schematic of electrospinning setup [19]

evaporation for solution electrospinning, thereby influencing the diameter of the fiber.

Experimental design

From preliminary trials, a range of critical material attribute (CMAs) and critical process parameters (CMAs) were derived and studied using 2^{5-2}fractional factorial design to check their effect on derived critical quality attributes. All independent variables were chosen at their two levels, (− low level) and (+, high level) [20], respectively. Table (1) shows the design variables specification.

Evaluation of design batches

Morphological structure of NFs SEM (JSM 6010 LA, JEOL, USA) technique was utilized to check the morphology and to measure fiber diameter of prepared NFs. The NFs were gathered and mounted on a twofold sided stick tape over aluminum stubs to get a uniform NFs sheet. NFs sample was platinum covered for 20 s. The conductive metal coating in the sample avoids heating, decreases thermal disruption and increases topographic interpretation of the SEM's secondary electron signal. Samples were observed, respectively, at 5 kV, 10 kV, 20 kV and images recorded [17, 18].

Tensile strength Mechanical properties of prepared NFs were characterized using the Instron-3365 (Instron Corporation, Norwood, MA, USA) universal testing method. The NFs were cut to (5 cm × 5 cm) in this test. Until breakage, the sample was placed

Table 1 The design variables specification

Independent variables	Levels (actual value)	
	Low (−)	High (+)
Concentration of MC (%) (X1)	1	1.5
Concentration of PVA (%) (X2)	8	10
Applied Voltage (kv) (X3)	20	25
Distance (cm) (X4)	10	15
Flow rate (ml/hr) (X5)	0.5	1
Dependent variables	*Target Value*	
Fiber diameter (Y1)	100–200 nm	
Tensile strength (Y2)	1–3 Mpa	
Controlled variables		
Syringe diameter	17 mm	
Syringe needle	18 gauge	
Solvent ratio	75:25 (Water: IPA)	

in the grips and stretched with a strain rate of 10 mm/min. Averages of Young's elasticity module (E), ultimate tensile strength (UTS) and break elongation (πb) were determined from stress–strain curves [23, 24].

Statistical analysis of design batches

Design Expert ® 9.0.6 Software was used for data optimization [25].

Model (polynomial equation) and significance

The Model additionally helps with segregating among significant and non-significant factors. The polynomial equations can be utilized to reach determinations relying upon the size of the co-sign and the experimental (positive or negative) image that it bears. In present analysis, linear polynomial equation was used to derive the effect of significant factors on response measured. When constructing a model using Experiment Model, the value p is always implied. $p < 0.05$ (at a 5% confidence interval) is deemed statistically important for a different model term [26].

ANOVA and response surface plot

One-way variance analysis (ANOVA) can be used to check the significance of the terms in the model. Model values F and values p were used to derive the outcome. The surface methodology was used to explain the relationship of three variables for surface plots in 2D and 3D model architecture. The x-and y-scales show independent variables and a smooth surface determined response (z) [27, 28].

Pareto chart

Pareto diagram is a graphical tool that represents the most significant variables. It is a vertically structured presentation wherein the bar-formed qualities '*t*' is plotted in diminishing requests of relative recurrence from left to right. The tallness of each bar shows the estimation of the property. The outline shows the level shaft for the various factors [29].

Selection of formulation with desirability function

Implementing the desirability function integrates all the solutions into one equation and offers the potential for independent variables to approximate optimum values. Measuring each desired functions involves combining the responses into one desirable function [24].

Characterization of NFs

FT-IR spectroscopy of NFs

FTIR analysis was carried out to validate the cross-linking between MC and PVA. For this study, (KBr) pellets were prepared using the homogeneously dried formulation and packed under vacuum utilizing round level face punch to make minimal pellets. The FT-IR NFs spectra were acquired utilizing FTIR (NICOLET-6700, Thermo Science, US) with an assimilation range of 4000–400 cm^{-1} [30].

Thermal method of analysis

The thermal method of analysis was employed to assess NFs thermal decomposition. Thermogravimetric analysis (TGA) and differential calorimetric scanning (DSC) (Mettler Toledo, Schimadzu, Japan) analysis were carried out at a temperature range of 30–500 °C at a heating rate of 10 °C min^{-1} in the nitrogen atmosphere [31].

X-ray powder diffraction (XRD)

The pattern of NFs X-ray diffraction ((Bruker, D2 Phase) was performed and compared with reference spectra of X-ray diffraction scans which carried out from 10° to 30° (2θ) at a scan rate of 2°/min using Ni-filtered Cu radiation. The diffraction pattern was used to measure the crystalline phases and their structural properties [32].

Atomic force microscopy (AFM)

The surface morphology of the NFs was described by a multimode IIIa AFM (Digital Instruments) and a dimension 3100 AFM (VEECO). For atomic force

microscopy (AFM) imaging, a touch mode was used. Using the integrated optical microscope, the cantilever was placed atop the NFs within micrometer precision. The data were obtained by mapping the 20 μm^2 grid size of the NFs. The cantilever tip deflection was used as a feedback signal to maintain a steady force over the area being tested. In touch force calibration mode, AFM force-versus-distance curves check the mechanical properties of the NFs [33].

Contact angle study

A measuring tool (GBX DIGIDROP) was used to determine the hydrophilic/hydrophobic character of the NFs. Using a syringe, a drop of water (1 µL) was collected on the surface of NFs. As droplets are produced on the water, a video camera used to take an image of the falls. The touch angle for each sample was determined to mitigate experimental error at three different sites, and then the average was recorded [34].

Rate of biodegradation

The integrity of NFs under environmental elements during production, storage, transportation, and usage is an important factor for the application. To investigate this rate of biodegradation study was performed. At an average weight of 3 mg, the NFs were cut in (2 cm × 2 cm) and soaked at 37 °C with 10 mL PBS. The residual sample was carefully drained from the well at a set time intervals (1, 3, 5, 7 days), rinsed with deionized water, dried at 60 °C until the weight remained unchanged and then measured. The percent mass loss was plotted vs. time to get the NFs degradation profile [35, 36].

The mass loss percentage has been calculated using the following equation:

$$WL = \frac{wi - wt}{wi} \times 100$$

where WL is the sample mass loss percentage, and wi is the dry sample initial weight, wt is the dry sample weight at any given time (1, 3, 5, 7 days).

Evaluation of antimicrobial property

A NFs mat demonstrated an antimicrobial property for topical applications to eliminate direct infections. Henceforth, to check the antibacterial activity of NFs, the growth inhibition of *E. coli* was observed. Briefly, 200 µl of Fluid Thioglycolate medium pH 7.1 and Soybean Casein Digest Medium, pH 7.3 was added to (0.5×0.5) cm^2 of each scaffold in a 96 well tissue culture plate with 1×107 CFU/ml bacterial inoculum and incubated for 24 h at 37 °C. After removing planktonic cells from the wells each of the NFs was washed with PBS solution (pH 7.4). 0.1% of crystal violet solution was then added into the wells (100 µl per wells) and incubated

for 20 min at room temperature. After removal of crystal violet solution, samples were again washed thrice with PBS solutions and destained with absolute ethanol. The bacterial growth inhibition was monitored through spectrophotometer measurements at 570 nm [37, 38].

Results and discussion

Fabrication of NFs

Screening of solvent

Preliminary trials were carried out using plain MC. Varied concentration of MC (%w/v) solution was prepared for observation of NFs morphology in solvent blend ratios. Preliminary results of the batches are shown in Table 2.

From the preliminary trials, uniform and stable fibers were observed in water-to-IPA (75:25) solvent ratio. NFs was observed in water-to-IPA ratio due to solubility of polymers in preferred solvents for electrospinning processes and its moderate boiling point. Generally, volatile solvents are selected because their high rate of evaporation facilitates the easy evaporation of the solvent from the NFs during their flight from the tip of the needle to collector. However, extremely soluble solvents are often avoided because their low boiling points and high rate of evaporation allow the jet to settle at the tip of the nozzle. This drying would obstruct the tip of the needle and thereby hinder the cycle of electrospinning. Similarly, less volatile solvents are also avoided because of their high boiling points during NFs jet flight prevent their drying out [39]. Tensile strength of observed fibers was found to be 0.0820 Mpa which was considered very weak for the application of drug delivery. Further attempt was made to obtain desired mechanical properties combining appropriate polymer. Different experiments were performed using a specific polymer approved by the FDA, and results are shown in Table 3. Figure 2 displays SEM images of MC in the water to IPA solvent ratio of 75:25 at high and low magnifications (Fig. 3).

Screening of co-blend polymer with MC

To obtain desired mechanical properties screening of polymer with MC concentration 1.5% in water to IPA ratio 75:25 was carried out. The results for the test batches are shown in Table 3.

The formation of uniform and stable fibers with PVA in a concentration range of 8–10% w/v was observed with MC in concentration of 1.5% in water to IPA ratio 75:25. Therefore, further study of NFs fabrication was carried out using MC and PVA blend in a concentration of 10% w/v and 1.5% w/v, respectively (Fig. 4).

Table 2 Preliminary batches composition of MC with various blends of solvents

Trial batch	Concentration	Solvent ratio	Remarks
P1	1.0	Water: Ethanol (1:1) ratio	No fibers were observed. Due to high dielectric constant of water droplets were observed on collector disk. Therefore in further batches water was taken in fewer amounts
P2	1.2		
P3	1.4		
P4	1.5		
P5	1.0	Water: Acetone (1:1) ratio	No fibers were formed due to high volatility of solvent water droplets were observed on collector disk
P6	1.2		
P7	1.4		
P8	1.5		
P9	1.0	Water: IPA (1:1) ratio	Fibers were observed in 1.5 concentration of MC with (1:1) ratio of water and IPA. Further trial was conducted with different ratios of water and IPA in order to get stable and uniform fibers with proper thickness
P10	1.2		
P11	1.4		
P12	1.5		
Methyl cellulose (1.5% w/v) in different ratio of Water: IPA ratio			
P13	1.5	Water: IPA ratio (75:25) solvent ratio	Uniform and stable fibers were observed
P14	1.5	Water: IPA ratio (50:50) solvent ratio	Fibers with irregular beads observed
P15	1.5	Water: IPA ratio (60:40) solvent ratio	Fibers with irregular beads observed

Table 3 Screening results of polymer with MC concentration 1.5% w/v

Trial batches	Conc. of polymer (% w/v)	Fiber diameter (nm) (Mean ± SD)	Morphology	Conclusion
PVA in (75:25 Water: IPA) ratio of solvent				
P17	2%	360 ± 1.2	Fibers with beads	NFs containing blend of Methyl cellulose and PVA is having good mechanical strength and uniform fibers
P18	4%	250 ± 2.2	Fibers with beads	
P19	6%	400 ± 1.3	Fibers with beads	
P20	8%	320 ± 2.5	Uniform distribution of fibers without beads	
P21	10%	200 ± 3.3	Uniform distribution of fibers without beads	
P22	12%	520 ± 3.1	Non Uniform distribution of fibers with beads	
PVP in (75:25 Water: IPA) ratio of solvent				
P23	2%	300 ± 1.1	Single fibers	Uniform fibers were observed in 2% and 4% concentration of PVP but mechanical strength is low
P24	4%	350 ± 1.2	Single fibers	
P25	6%	400 ± 3.3	Single fibers	
P26	8%	299 ± 3.1	Single fibers	
P27	10%	500 ± 3.5	Single fibers	
P28	12%	456 ± 2.2	Single fibers	
PCL in (75:25 Water: IPA) ratio of solvent				
P29	1%	960 ± 1.2	Uniform fibers was observed	Uniform fibers were observed but fiber diameter is large
P30	1.5%	1121 ± 1.3	Uniform fibers was observed	
P31	2%	800 ± 1.5	Uniform fibers was observed	
P32	2.5%	960 ± 1.3	Uniform fibers was observed	
Chitosan in (75:25 Water: IPA) ratio of solvent				
P33	1%	150 ± 1.5	Single fibers	Formation of irregular fibers with regular beads
P34	1.5%	175 ± 1.1	Single fibers	
P35	2%	250 ± 1.3	No uniform fibers	
P36	2.5%	380 ± 1.2	No uniform fibers	

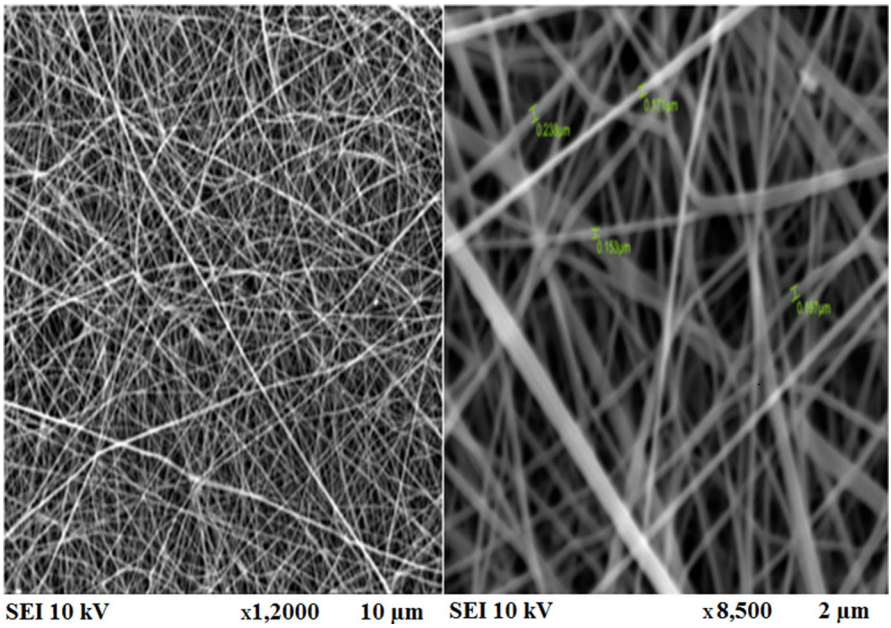

Fig. 2 SEM images of MC in 75:25 ratio of water to IPA solvent

Identification of process and formulation parameters by screening design

The process and formulation parameters were defined and screened using 2^{5-2} fractional factorial design from the preliminary batch results and literature studies. A total of 11 experimental runs were performed in 2^{5-2} fractional factorial architecture. Table 4 displays the structure of batches along with outcomes for dependent variables (Fig. 5).

Morphological structure of NFs

Figure 6 shows the morphology and fiber diameter of an optimized batch of nanofibers. SEM evaluation revealed that the formation of uniform NFs with random orientation.1.5% w/v concentration of MC NFs mat shows the uniform fiber with diameter range 100–250 nm ± 2.1 nm. 10% w/v concentration of PVA NFs mat shows the uniform fiber with diameter range 100–250 nm ± 3.3 nm. The fiber of 1.5% w/v concentration of MC co-blended with 10% w/v concentration of PVA shows the uniform fiber with diameter 100–166.6 ± 1.1 nm size. It was observed that flow rate, applied voltage, distance and concentration of polymer had great effect on fiber diameter and morphology [40].

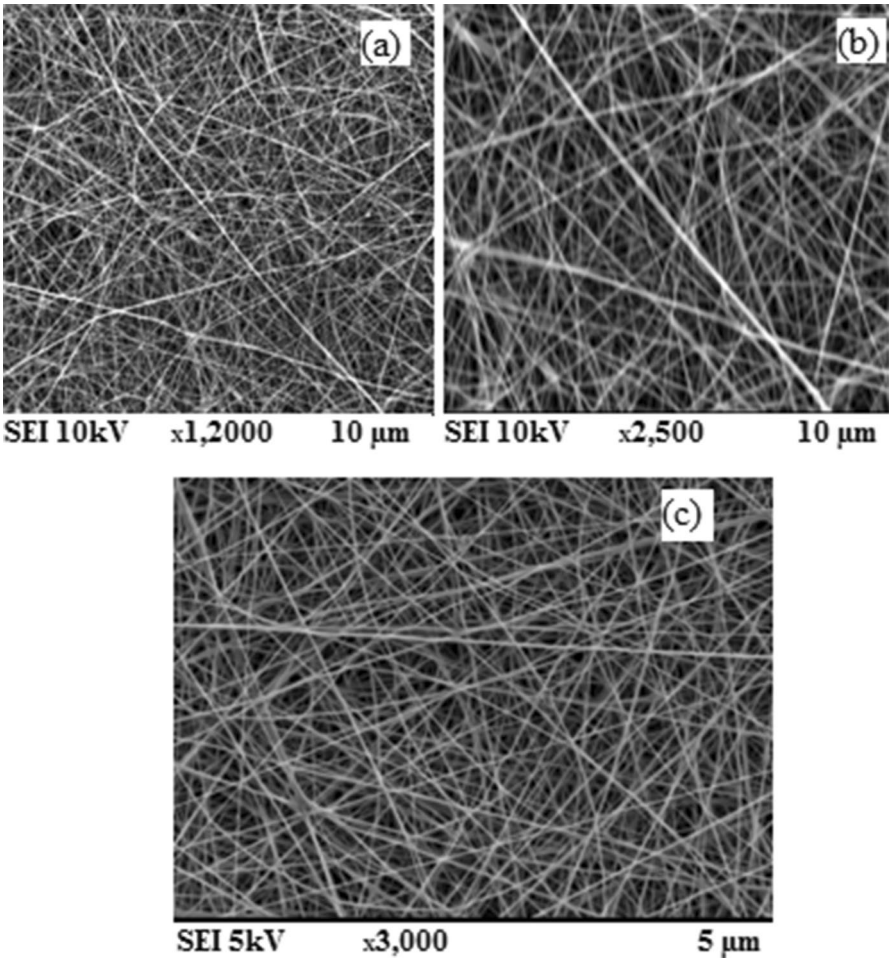

Fig. 3 SEM images of **a** 1.5% w/v MC NFs, **b** 10% w/v PVA NFs, **c**1.5% w/v MC co-blended with 10% w/v PVA NFs

Tensile strength of NFs

Figure 4 displays the stress–strain curves of MC NFs, PVA NFs and MC with PVA NFs. Table 5 indicates the elongation values at the break and ultimate tensile power. MC NFs tensile strength was observed up to 0.082 Mpa, and PVA NFs were observed up to 2.09 Mpa and increased tensile strength was observed in MC mixture with PVA up to 2.74 Mpa suggesting desired mechanical strength for drug delivery application. As observed in figure loading PVA with MC resulted in a strong effect favored by increased interfacial area and more active surface compared to NFs from MCNFs. In comparison with MC NFs and PVA NFs, the elasticity modulus of MC with PVA NFs

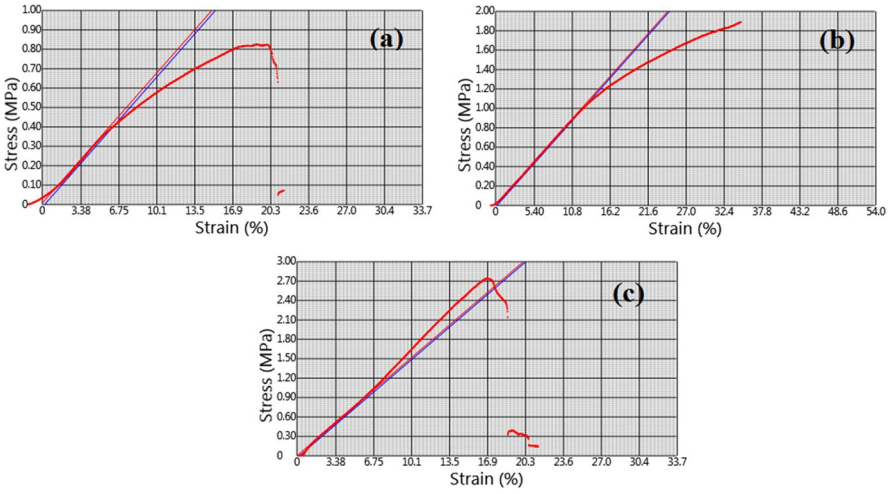

Fig. 4 Tensile strength of NFs Tensile strength of **a** MC NFs **b** PVANFs **c** MC + PVA NFs

was increased. Improvement of MC NFs mechanical properties with PVA NFs resulted from strong matrix interface adhesion. The key explanation for improved adhesion between the phases is the hydrogen bonding between –OH group of MC fibers and a similar group of PVA fibers that resulted in improved mechanical properties [41, 42].

Analysis of design batches using software

Software

The effect of each variable on the designated response was analyzed by software Design Expert® 9.0.6.

Model (polynomial equation) and significance

The specification for the screening of MC, the concentration of PVA, applied voltage, distance and flow rate showed a significant effect on fiber diameter and tensile strength. Through the fractional factorial design of 2^{5-2} these important factors were further optimized.

Table 6 displays the independent variables and the dependent variables (fiber diameter, tensile strength) for screening batches. Effect of independent variables such as concentration of MC (% w/v) (A), concentration of PVA (% w/v) (B), Applied voltage (kV)(C), Distance (cm) (D) and Flow rate ((ml/hr) (E) on dependent variables fiber diameter and tensile strength are shown in Figs. 5, 6 in form of plots of the response surface. Fiber diameter shows a range of 150 ± 1.1 nm to 350 ± 4.7 nm. The

Table 4 Results of screening design experimental batches

Batch	Conc. of MC	Conc. of PVA	Applied voltage (kV)	Distance (cm)	Flow rate (ml/hr)	Fiber diameter (nm) (Mean ± SD)	Tensile strength (Mpa) (Mean ± SD)
F1	1	8	20	15	1	205.1 ± 4.7	1.85 ± 0.2
F2	1.5	8	20	10	0.5	150.4 ± 6.4	1.72 ± 0.1
F3	1	10	20	10	1	324.5 ± 3.6	2.65 ± 0.1
F4	1.5	10	20	15	0.5	228.6 ± 1.2	2.55 ± 0.2
F5	1	8	25	15	0.5	168.6 ± 3.3	1.82 ± 0.1
F6	1.5	8	25	10	1	137.6 ± 5.3	1.11 ± 0.3
F7	1	10	25	10	0.5	275.3 ± 2.5	2.69 ± 0.3
F8	1.5	10	25	15	1	166.6 ± 1.1	2.74 ± 0.2
F9-F11	1.25	9	22.5	12.5	0.75	183.3 ± 1.2	2.06 ± 0.1

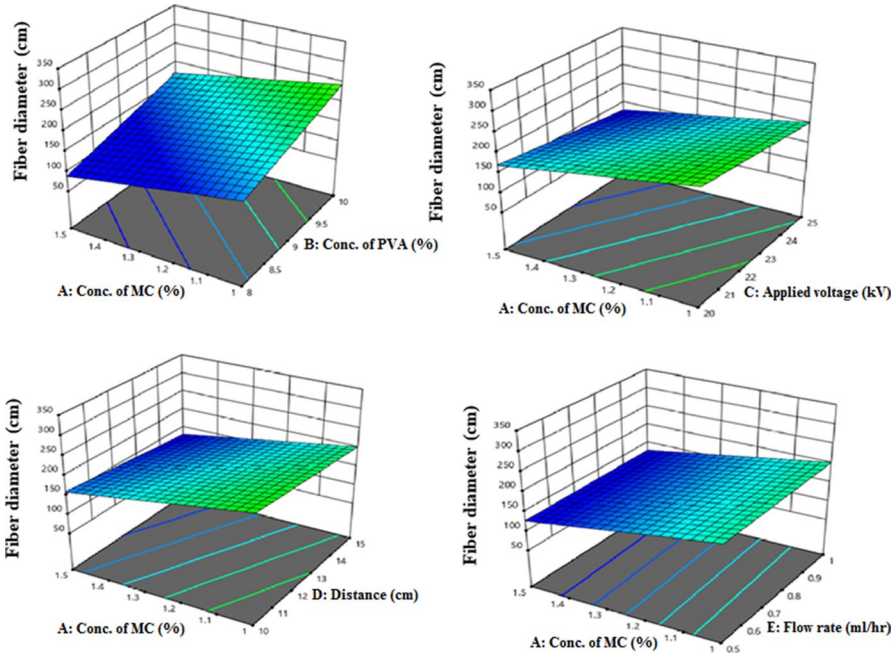

Fig. 5 Response surface 3D plot for Fiber diameter [Y1]

Tensile strength shows a range of 0.82 ± 0.01 Mpa to 2.74 ± 0.1 Mpa. This means independent variables such as A, B, C, D, E play an important role in altering fiber diameter and tensile strength. It was found from Table 6 polynomial equations that conc. of MC (w/v percentage) (A), conc. of PVA (percentage w/v) (B), applied voltage (kV)(C), distance (cm) (D) and flow rate (ml/hr) (E) less than ($p > 0.05$) show major effect on the fiber diameter and tensile strength.

ANOVA was applied to estimate the model's value at a point of 5 percent. The results of which the variance analysis (ANOVA) was performed to check the significance of the quadratic models and the lack of fit for the experimental data are summarized in Table 7.

Response surface plot

The fiber diameter and tensile strength response plot of MC with PVA NFs for experimental factors are shown in Figs. 5, 6. Figure shows the effect of MC, PVA, applied voltage, distance and flow rate on fiber diameter and tensile strength. It has been observed that fiber diameter and was improved with increases in the concentration of MC and PVA. It has also been found that an increase in applied voltage increases the diameter of fibers. It has been observed that increases in the distance lead to the finest fiber diameters and also decreases the number of beads. From the graph, it was found that the fiber diameter often increases as the flow rate increases. Figure 6 demonstrates the effect on the tensile strength of the independent variables.

An increased concentration of MC and PVA results in increased tensile strength was observed from the graph. It was also found that the applied voltage rise also increases the tensile power. It has been observed that a rise in distance and flow rate indicates an increase in tensile strength.

Pareto chart

The Pareto chart displays individual values of the significant factors represented by bars from left to right in descending order, and the cumulative sum shown by

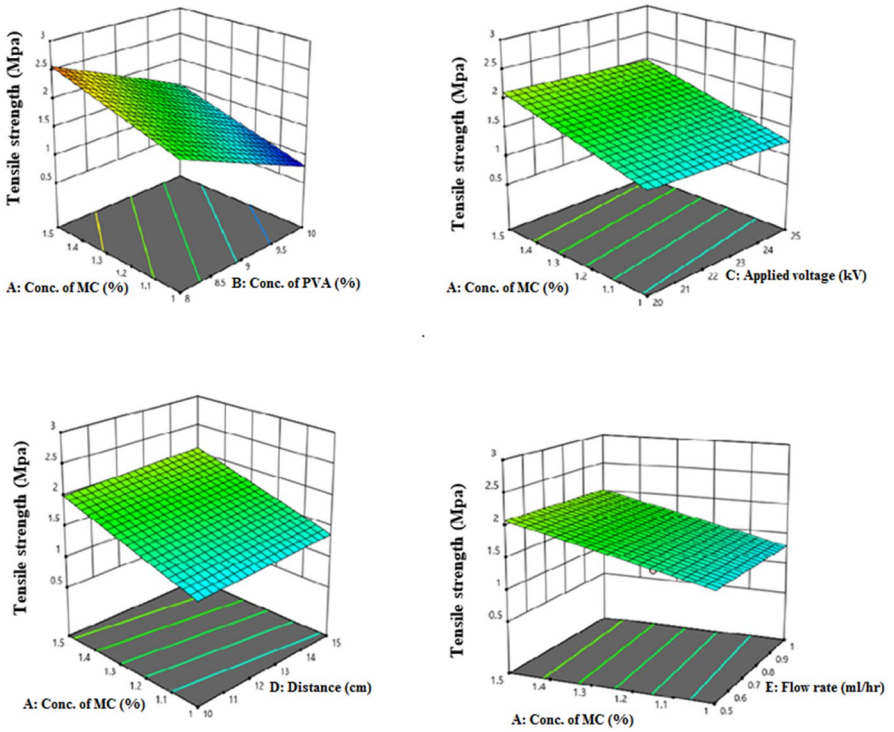

Fig. 6 Response surface 3D plot for Tensile strength [Y2]

Table 5 Results of tensile strength of electrospun NFs

Sample	Thickness (mm)	Tensile strength (Mpa)	Modulus of elasticity (Mpa)
MC NFs	0.49	0.082	6.59
PVA NFs	1.01	2.09	11.9
MC + PVA NFs	1.49	2.74	14.9

Table 6 Result of regression analysis with respect to fiber diameter and % EE (2^{5-2} fractional factorial design)

Independent variables	*A*	*B*	*C*	*D*	*E*
Regression analysis					
Coefficients (*p* value) of fiber diameter	−36.32	41.695	−20.08	−14.895	1.38
	p (0.0027)	*p* (0.0014)	*p* (0.0282)	*p* (0.0726)	*p* (0.8412)
Coefficients (*p* value) of Tensile strength	−0.0800	0.5050	−0.0500	0.0888	−0.0850
	p (0.3884)	*p* (0.0019)	*p* (0.5807)	*p* (0.5448)	*p* (0.3618)
Polynomial equation					
Fiber diameter $= +201.07 - 36.32 * A + 41.70 * B - 20.08 * C - 14.90 * D + 1.38 * E \left(R^2 = 0.9447\right)$					
Tensile strength $= +2.11 - 0.0800 * A + 0.5050 * B - 0.0500 * C + 0.0500 * D - 0.0850 * E \left(R^2 = 0.9891\right)$					

Table 7 ANOVA analysis for measured responses

Response	Source	Degree of freedom	Sum of square	Mean sum of square	*F* ratio	*P* value	Remarks
Fiber diameter [Y1]	Model	5	29,476.70	5895.34	17.08	< 0.0037	Significant
	Residual (error)	5	1725.66	345.13	–	–	–
	Total	10	31,202.36	–	–	–	–
Tensile strength [Y2]	Model	5	2.19	0.4387	7.64	< 0.0218	Significant
	Residual (error)	5	0.2871	0.0574		–	–
	Total	10	2.48	–	–	–	–

the rows. The height of each bar determines the value of the variables as shown in Fig. 7. It was observed that conc. of PVA, conc. of MC applied voltage and distance has a major effect on fiber diameter based on greater t-value. From the Pareto chart it was found that conc. of PVA and conc. of MC has a major effect on tensile strength due to greater t-value.

Optimization of formulation with desirability function

For calculating desirability value, software was assigned command with respect to least fiber diameter and tensile strength. Software predicted optimized batch having desirability value of 0.979 was observed from the desirability graph (Fig. 8).

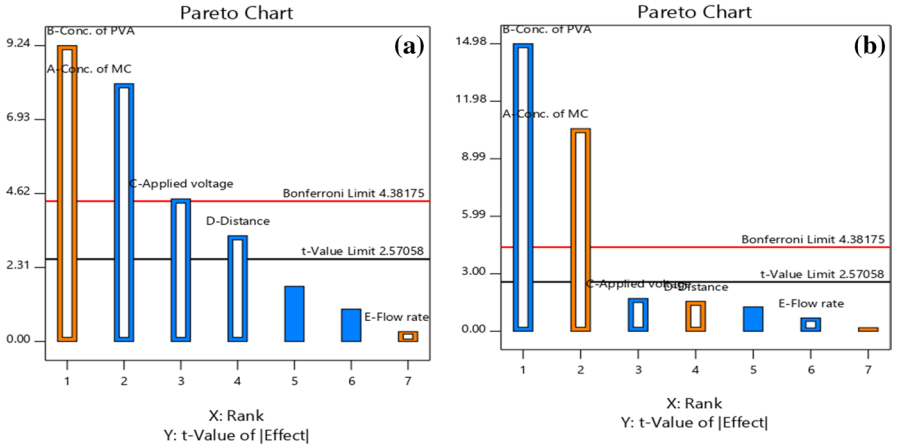

Fig. 7 Pareto Chart of independent variables on **a** fiber diameter and **b** tensile strength

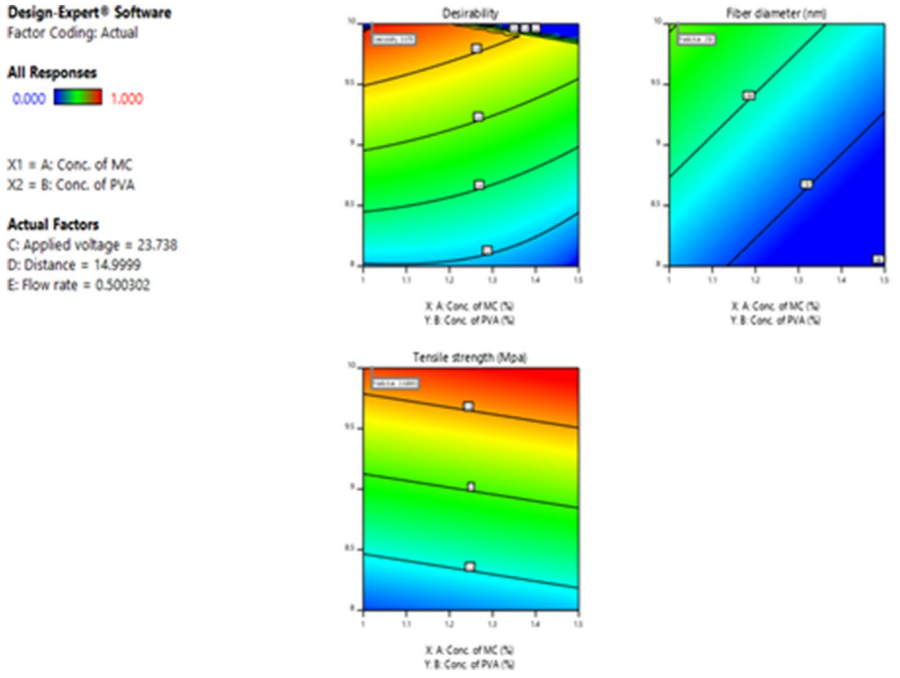

Fig. 8 Desirability plot of optimized batch

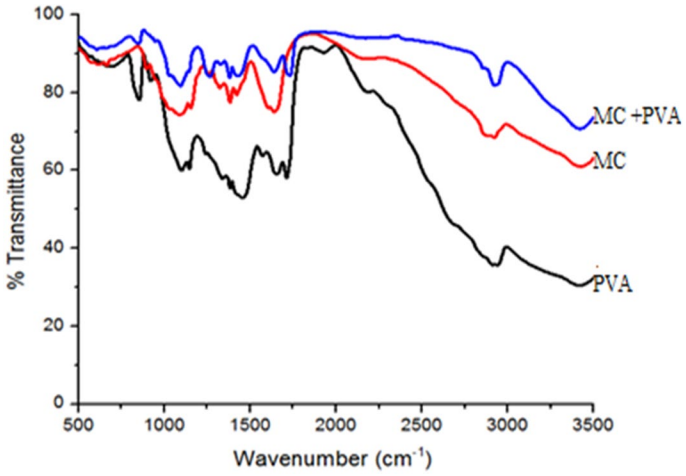

Fig. 9 FTIR images of optimized batch on **a** PVA **b** MC and **c** MC with PVA NFs

Characterization and evaluation of NFs

FTIR spectroscopy of NFs

The wide peak at 3700–3584 cm^{-1}shows O–H stretching intermolecular and intramolecular hydrogen bond in MC NFs, and C-H aliphatic stretching vibrations in MC NFs are linked to 3000–2840 cm^{-1}. The peak at 892.19 cm^{-1} is a characteristic MC peak that demonstrates the linkage in MC structure that is held together with H-bonds. The basic composition of PVA is-(CH2 –CHOH)n and the structure of the monomer is (CH2 = CHOH). Figure 9 clearly shows the important PVA related peaks. The peak observed at approximately 1147.48 cm^{-1} is attributed to the presence of terminal PVA groups and 1466 cm^{-1} indicates the –C=O carbonyl stretching bond. It is observed that the band obtained at 2810–3000 cm^{-1} indicates C-H stretching bond and the peak at 3200–3870 cm^{-1} is hydrogen bonded –OH group.

From the spectra of MC with PVA broad peak at 3313.95 cm^{-1} of O–H stretching vibration from the intermolecular and intramolecular hydrogen bond in MC and PVA structures. The peak at 2927.57 $cm^{-1}$is attributed to C-H aliphatic stretching vibration in MC and C-H from the alkyl group of PVA. At 1163 cm^{-1} the peak is attributed for the assessment tool of PVA structure because it is a semi-crystalline synthetic polymer able to form some domains. The peak at 768.66 cm^{-1} is a characteristic peak of MC which shows the linkage held together with H-bonds in MC structure. The spectra clearly indicate the stronger relationship between PVA and MC with small changes from the standard spectrum of PVA [43, 44].

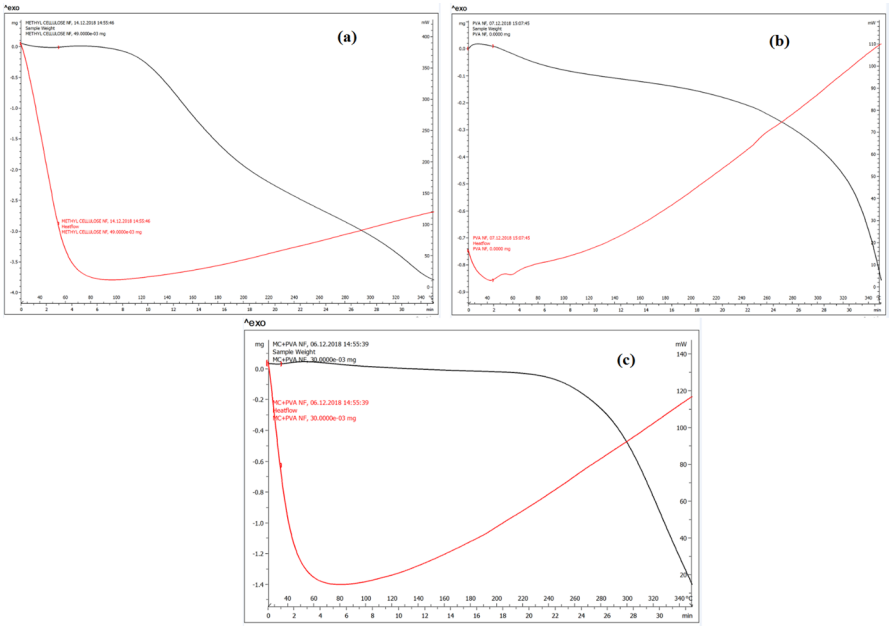

Fig. 10 DSC-TGA analysis graphs of **a** MC NFs **b** PVA NFs **c** MC with PVA NFs

Thermal method of analysis

TGA is mainly used to investigate the thermal stability of polymers. Most polymers melt or degrade before 200 °C. However, there is a class of thermally stable polymers that are able to withstand temperatures of at least 300 °C in air and 500 °C in inert gases without structural changes or strength loss, which can be analyzed by TGA.DSC-TGA diagram of MC with PVA NFs has appeared in Fig. 10, the glass transition temperature (Tg) of MC with PVA NFs is lower compared with plain MC and PVA NFs, this might be because of the closeness of flexible side gatherings (alkyl) of MC which increment the separation between chains in the blend and lessening the interchain associations causing a diminishing in Tg esteem. Figure 10, it very well may be demonstrated that the endotherm of the water stream happens in the scope of 80 °C and 100 °C. This endotherm is available on the thermogram of cellulosic matter as indicated by the water association and the non-subbed hydroxyl gatherings of cellulose subordinates. The pure PVA fibers displayed a relatively wide and straight endothermic curve with a peak of 196 °C. Nonetheless, the value for the cross-linked PVA NFs shifted toward the low temperature. The glass transition temperature (Tg) for MC is 60 °C with PVA, respectively. Therefore it can be concluded that the thermal properties are ideal for drug delivery applications [45].

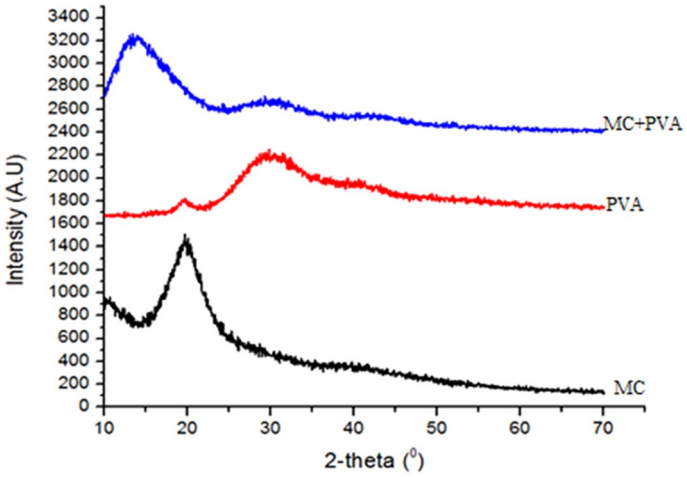

Fig. 11 XRD Graph of NFs (MC NFs, PVA NFs and MC with PVA NFs)

XRD graph of NFs

Figure 11 displays XRD spectra of MC NFs, PVA NFs and MC co-blended with PVA. XRD spectra of MC NFs display peak characteristics at 20.9θ and PVA NFs display peak characteristics at 32.8θ. XRD spectra of MC co-blended with PVA show characteristic peak at 14.9θ, it indicates the semi-crystalline nature of the formulation due to the occurrence of heavy intermolecular and intramolecular hydrogen bonding [37, 40].

Atomic force microscopy of NFs

Figure 12 displays the AFM images of MC co-blended with PVA NFs, respectively. The findings show that due to the convolution of the tip outline with NFs geometry the diameter of the fibers obtained by AFM was extended form. The morphology of NFs prepared from MC concentration of 1.5% w/v co-blended with PVA concentration of 10% w/v reveals the thick matrix of standard fibers with significantly improved surface roughness. Both SEM & AFM findings will direct the identification of optimal conditions for synthesizing NFs of this form [19, 41].

Contact angle of NFs

Figure 13 shows the water contact angles for MC NFs, PVA NFs, and MC co-blended with PVA NFs. The mats are hydrophilic when the contact angle is less than 90°, so the lower contact angle is the stronger hydrophilicity. Conversely, the mats become hydrophobic when the touch angle is greater than 90°. Figure 13 shows the images of 1 µL water droplets that live on the electrospun NFs mats surface. The MC and PVA NFs water touch angles are 27.22° (Fig. 13a)

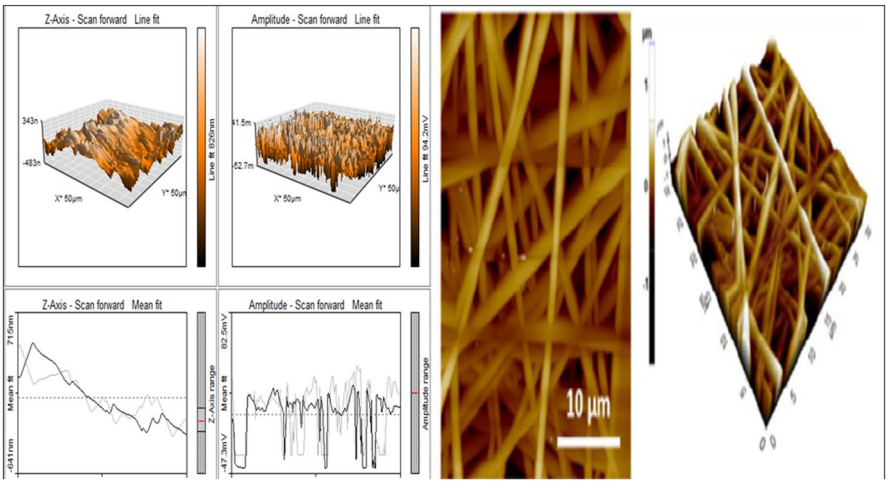

Fig. 12 AFM images of MC with PVA NFs

and 48.73°, respectively (Fig. 13b). On the surface of MC and PVA NFs mats the water droplet had a lot of spread. Figure 13c shows a good hydrophilicity contact angle of (62.40°), which clearly indicates that the addition of PVA and MC improves wettability of prepared NFs. Such values were averaged from five samples at different locations of the sheet, suggesting that the MC, PVA and MC with PVA NFs dispersed equally and formed the high porosity blend NFs that resulted in a hydrophilic surface [48].

Rate of biodegradation

Figures 14and 15 show the rate of biodegradation of MC, PVA, and MC with PVA NFs. The PVA NFs, MC with PVA NFs had the highest degradation resistance because they retained their initial weight after a week. In the case of MC with PVA NFs, the percentage of mass loss was reduced with time intervals up to the seventh day. Most of the fibers were swollen and part of the fibers broken down after 7th day incubation in PBS 7.4. The composition of the NFs was found with a minimal amount of minor cracks and voids. The smaller fiber diameter of the NFs will increase the NFs 'surface-to-volume ratio and the degradation rate [37, 42]. These indicate good integrity of the NFs for long-term use in the human body condition, an importance requirement on dressing materials.

Antimicrobial property

Spectrophotometric measurements after antimicrobial evaluation of different NFs samples show that bacterial cells adhered readily onto the surface of MC (Fig. 16).

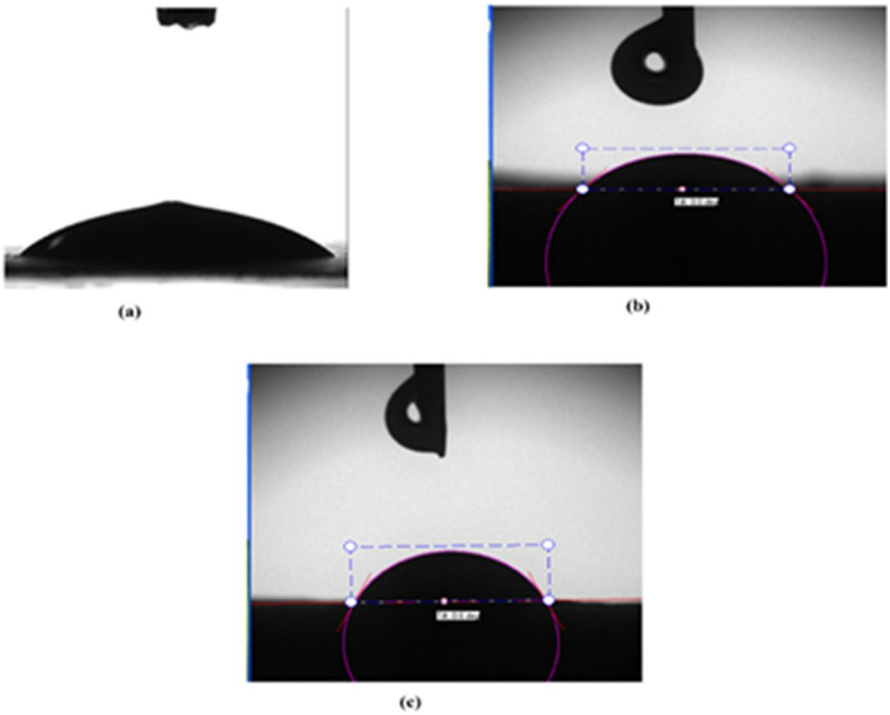

Fig. 13 Contact angle of **a** MC NFs **b** PVA NFs mat and **c** MC PVA NFs mat

However, the reduced optical density of PVA NFs and MC-PVA NFs, indicates less bacterial adhesion on it compared to MC NFs only. The reduction in cell adhesion for MC-PVA NFs may be explained by antibacterial nature of PVA that inhibits the permeability of negatively charged bacterial cell through positively charged functional groups of PVA. Enhanced inhibition ability against the growth of *E. coli* for MC-PVA NFs clearly ensures its potential as an ideal substitute for drug delivery application [37, 38].

Conclusion

In summary, the fabrication of NFs was done using MC with PVA as co-blended polymers using the electrospinning method. Optimized NFs showed excellent biocompatibility, biodegradable properties, non-toxicity, and ease of solubility in commonly used organic solvents for pharmaceutical application. Effect of formulation and processing variables was studied to get critical quality attributes like fiber diameter and tensile strength. Further, the prepared formulation was characterized by SEM, tensile strength, FTIR, DSC-TGA, XRD, AFM, Contact angle, and rate of

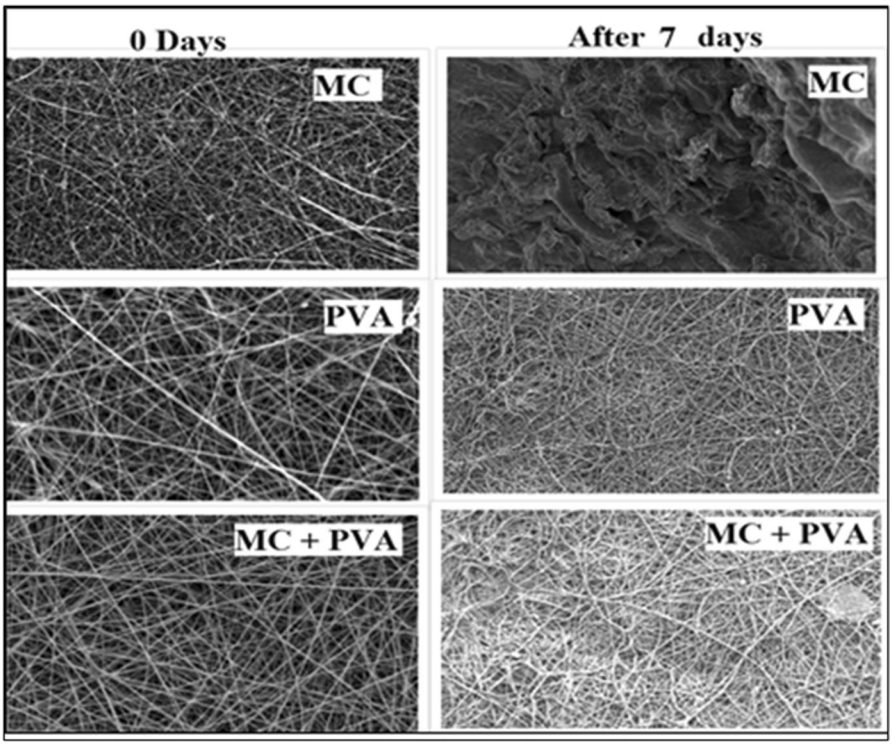

Fig. 14 SEM images MC, PVA and MC with PVA NFs after 7thday's incubation in PBS

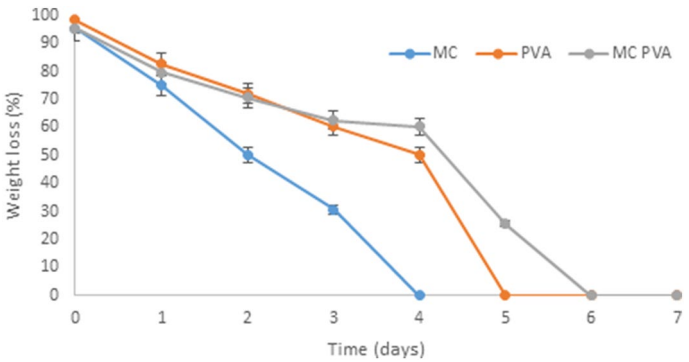

Fig. 15 Biodegradation study graph of MC NFs, PVA NFs, and MC with PVA NFs

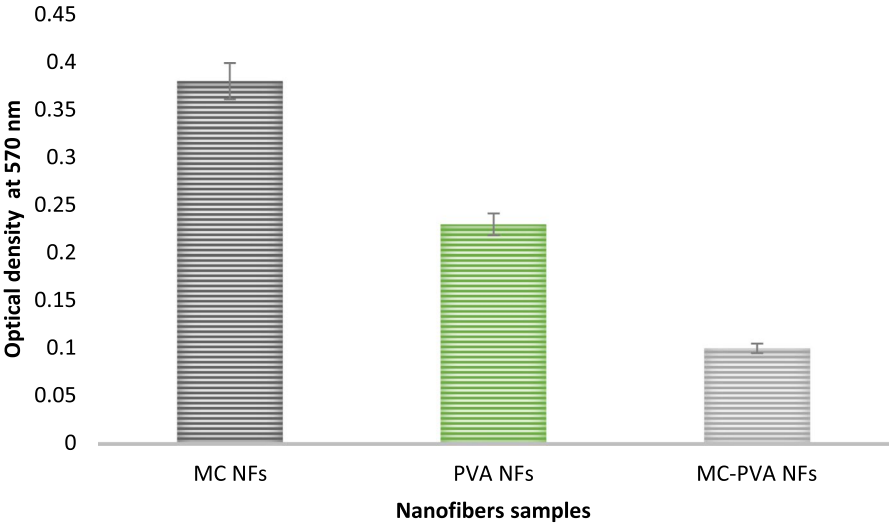

Fig.16 Optical densities measured for electrospun NFs after exposing to *E. coli*

biodegradation. An antimicrobial study was also carried out to prove the potential of prepared NFs. The test of assessment and characterization demonstrated strong polymer compatibility into prepared NFs. Overall, all findings in the present research work suggest the potential use of MC with PVA NFs for drug delivery applications like topical.

Acknowledgement The authors are thankful to Ramanbhai Patel College of Pharmacy, Charotar University of Science and Technology (CHARUSAT) for extended financial support to carry out this research work.

Funding Declared none.

Declarations

Conflict of interest The authors declare that they have no conflict of interest.

Consent for publication Not applicable.

References

1. Sofi HS, Abdal-hay A, Ivanovski S (2020) Electrospun nanofibers for the delivery of active drugs through nasal, oral and vaginal mucosa: Current status and future perspectives. Mater Sci Eng 111:110756
2. Feng X, Li J, Zhang X et al (2019) Electrospun polymer micro/nanofibers as pharmaceutical repositories for healthcare. J Control Release 302:19–41
3. Venugopal J, Ramakrishna S (2005) Applications of polymer nanofibers in biomedicine and biotechnology. Appl Biochem Biotechnol–Part A Enzym Eng Biotechnol 125:147–157

4. Topuz F, Uyar T (2019) Electrospinning of cyclodextrin functional nanofibers for drug delivery applications. Pharmaceutics 11(1):6
5. Hu X, Liu S, Zhou G et al (2014) Electrospinning of polymeric nanofibers for drug delivery applications. J Control Release 185:12–21
6. Alghoraibi I, Alomari S (2018) Different Methods for Nanofiber Design and Fabrication. In: Handbook of Nanofibers. pp 1–46
7. Li S, Lee BK (2020) Electrospinning of circumferentially aligned polymer nanofibers floating on rotating water collector. J Appl Polym Sci. https://doi.org/10.1002/app.48759
8. Kurečič M, Smole MS (2013) Elektropredenje: Postopek izdelave nanovlaken. Tekstilec 56:4–12. https://doi.org/10.14502/Tekstilec2013.56.4-12
9. Chahal S, Hussain FSJ, Kumar A et al (2016) Fabrication, characterization and in vitro biocompatibility of electrospun hydroxyethyl cellulose/poly (vinyl) alcohol nanofibrous composite biomaterial for bone tissue engineering. Chem Eng Sci 144:17–29. https://doi.org/10.1016/j.ces.2015.12.030
10. Chahal S, Hussain FSJ, Yusoff MM et al (2017) Nanohydroxyapatite-coated hydroxyethyl cellulose/poly (vinyl) alcohol electrospun scaffolds and their cellular response. Int J Polym Mater Polym Biomater 66:115–122. https://doi.org/10.1080/00914037.2016.1190926
11. Guo JJ, Kelton CML (2016) Competition between brand name and generic drugs. In: Pharmaceutical Public Policy. pp 181–193
12. Dutta SD, Patel DK, Lim KT (2019) Functional cellulose-based hydrogels as extracellular matrices for tissue engineering. J. Biol, Eng, p 13
13. Yuwawech K, Wootthikanokkhan J, Tanpichai S (2015) Effects of two different cellulose nanofiber types on properties of poly(vinyl alcohol) composite films. J Nanomater. https://doi.org/10.1155/2015/908689
14. Mueller S, Sapkota J, Nicharat A et al (2015) Influence of the nanofiber dimensions on the properties of nanocellulose/poly(vinyl alcohol) aerogels. J Appl Polym Sci. https://doi.org/10.1002/app.41740
15. Kenry LCT (2017) Nanofiber technology: current status and emerging developments. Prog Polym Sci 70:1–17
16. Lin CM, Chang YC, Cheng LC et al (2020) Preparation of graphene-embedded hydroxypropyl cellulose/chitosan/polyethylene oxide nanofiber membranes as wound dressings with enhanced antibacterial properties. Cellulose 27:2651–2667. https://doi.org/10.1007/s10570-019-02940-w
17. Eskitoros-Togay M, Bulbul YE, Dilsiz N (2020) Combination of nano-hydroxyapatite and curcumin in a biopolymer blend matrix: Characteristics and drug release performance of fibrous composite material systems. Int J Pharm. https://doi.org/10.1016/j.ijpharm.2020.119933
18. Patel GC, Yadav BK (2018) Polymeric nanofibers for controlled drug delivery applications. In: Organic Materials as Smart Nanocarriers for Drug Delivery. pp 147–175
19. Patel G, Yadav BKN (2019) Formulation, characterization and in vitro cytotoxicity of 5-fluorouracil loaded polymeric electrospun nanofibers for the treatment of skin cancer. Recent Pat Nanotechnol 13:114–128. https://doi.org/10.2174/1872210513666190314095643
20. Vora R, Shah Y (2019) Investigation of quality target process parameters and critical material attributes of nanocellulose as a potential excipient. Int J Appl Pharm 11:386–395
21. Deepa B, Abraham E, Cherian BM et al (2011) Structure, morphology and thermal characteristics of banana nano fibers obtained by steam explosion. Bioresour Technol 102:1988–1997. https://doi.org/10.1016/j.biortech.2010.09.030
22. Širc J, Hobzová R, Kostina N et al (2012) Morphological characterization of nanofibers: Methods and application in practice. J Nanomater. https://doi.org/10.1155/2012/327369
23. Baker SR, Banerjee S, Bonin K, Guthold M (2016) Determining the mechanical properties of electrospun poly-ε-caprolactone (PCL) nanofibers using AFM and a novel fiber anchoring technique. Mater Sci Eng C 59:203–212. https://doi.org/10.1016/j.msec.2015.09.102
24. Molnar K, Vas LM, Czigany T (2012) Determination of tensile strength of electrospun single nanofibers through modeling tensile behavior of the nanofibrous mat. In: Composites Part B: Engineering. pp 15–21
25. Sundarkrishnaa KL (2015) Design of experiments. Springer Ser Mater Sci 171:193–203. https://doi.org/10.1007/978-3-319-14069-8_5
26. Hinkelmann K (2012) Design and Analysis of Experiments
27. Anderson-Cook CM, Borror CM, Montgomery DC (2009) Response surface design evaluation and comparison. J Stat Plan Inference 139:629–641. https://doi.org/10.1016/j.jspi.2008.04.004

28. Mohamad Said KA, Mohamed Amin MA (2016) Overview on the response surface methodology (rsm) in extraction processes. J Appl Sci Process Eng. https://doi.org/10.33736/jaspe.161.2015
29. Keane AJ (2006) Statistical improvement criteria for use in multiobjective design optimization. AIAA J 44:879–891. https://doi.org/10.2514/1.16875
30. Ghosal K, Manakhov A, Zajíčková L, Thomas S (2017) Structural and surface compatibility study of modified electrospun Poly(ε-caprolactone) (PCL) composites for skin tissue engineering. AAPS PharmSciTech 18:72–81. https://doi.org/10.1208/s12249-016-0500-8
31. Saba N, Safwan A, Sanyang ML et al (2017) Thermal and dynamic mechanical properties of cellulose nanofibers reinforced epoxy composites. Int J Biol Macromol 102:822–828. https://doi.org/10.1016/j.ijbiomac.2017.04.074
32. Yan SH, Ma SY, Li WQ et al (2015) Synthesis of SnO2-ZnO heterostructured nanofibers for enhanced ethanol gas-sensing performance. Sensors Actuators B Chem 221:88–95. https://doi.org/10.1016/j.snb.2015.06.104
33. Johnson D, Oatley-Radcliffe DL, Hilal N (2017) Atomic Force Microscopy (AFM). In: Membrane Characterization. pp 115–144
34. Nadour M, Boukraa F, Ouradi A, Benaboura A (2017) Effects of methylcellulose on the properties and morphology of polysulfone membranes prepared by phase inversion. Mater Res 20:339–348. https://doi.org/10.1590/1980-5373-MR-2016-0544
35. Babaee M, Jonoobi M, Hamzeh Y, Ashori A (2015) Biodegradability and mechanical properties of reinforced starch nanocomposites using cellulose nanofibers. Carbohydr Polym 132:1–8. https://doi.org/10.1016/j.carbpol.2015.06.043
36. Song W, Markel DC, Wang S et al (2012) Electrospun polyvinyl alcohol-collagen-hydroxyapatite nanofibers: A biomimetic extracellular matrix for osteoblastic cells. Nanotechnology. https://doi.org/10.1088/0957-4484/23/11/115101
37. Chanda A, Adhikari J, Ghosh A et al (2018) Electrospun chitosan/polycaprolactone-hyaluronic acid bilayered scaffold for potential wound healing applications. Int J Biol Macromol. https://doi.org/10.1016/j.ijbiomac.2018.05.099
38. Croisier F, Atanasova G, Poumay Y, Jérôme C (2014) Polysaccharide-coated pcl nanofibers for wound dressing applications. Adv Healthc Mater. https://doi.org/10.1002/adhm.201400380
39. Haider A, Haider S, Kang IK (2018) A comprehensive review summarizing the effect of electrospinning parameters and potential applications of nanofibers in biomedical and biotechnology. Arab J Chem 11:1165–1188
40. Abd El-aziz AM, El-Maghraby A, Taha NA (2017) Comparison between polyvinyl alcohol (PVA) nanofiber and polyvinyl alcohol (PVA) nanofiber/hydroxyapatite (HA) for removal of Zn2+ ions from wastewater. Arab J Chem 10:1052–1060. https://doi.org/10.1016/j.arabjc.2016.09.025
41. Park Y, You M, Shin J et al (2019) Thermal conductivity enhancement in electrospun poly(vinyl alcohol) and poly(vinyl alcohol)/cellulose nanocrystal composite nanofibers. Sci Rep. https://doi.org/10.1038/s41598-019-39825-8
42. Peresin MS, Vesterinen AH, Habibi Y et al (2014) Crosslinked PVA nanofibers reinforced with cellulose nanocrystals: Water interactions and thermomechanical properties. J Appl Polym Sci. https://doi.org/10.1002/app.40334
43. Kumar A, Negi YS, Bhardwaj NK, Choudhary V (2012) Synthesis and characterization of methylcellulose/PVA based porous composite. Carbohydr Polym 88:1364–1372. https://doi.org/10.1016/j.carbpol.2012.02.019
44. Kanimozhi K, Basha SK, Kaviyarasu K, SuganthaKumari V (2019) Salt leaching synthesis, characterization and in vitro cytocompatibility of chitosan/poly(vinyl alcohol)/methylcellulose – ZnO nanocomposites scaffolds using L929 fibroblast cells. J Nanosci Nanotechnol 19:4447–4457. https://doi.org/10.1166/jnn.2019.16359
45. Kanimozhi K, Khaleel Basha S, Sugantha Kumari V (2016) Processing and characterization of chitosan/PVA and methylcellulose porous scaffolds for tissue engineering. Mater Sci Eng C 61:484–491. https://doi.org/10.1016/j.msec.2015.12.084
46. Kanimozhi K, Khaleel Basha S, Sugantha Kumari V et al (2018) In vitro cytocompatibility of chitosan/PVA/methylcellulose – Nanocellulose nanocomposites scaffolds using L929 fibroblast cells. Appl Surf Sci 449:574–583. https://doi.org/10.1016/j.apsusc.2017.11.197
47. Bhatnagar A, Sain M (2005) Processing of cellulose nanofiber-reinforced composites. J Reinf Plast Compos 24:1259–1268. https://doi.org/10.1177/0731684405049864

48. Kumar A, Negi YS, Bhardwaj NK, Choudhary V (2013) Synthesis and characterization of cellulose nanocrystals/PVA based bionanocomposite. Adv Mater Lett 4:626–631. https://doi.org/10.5185/amlett.2012.12482